JOURNAL OF COMPUTATIONAL PHYSICS **133,** 43–55 (1997)
ARTICLE NO. CP975644

Developing Numerical Fluxes with New Sonic Fix for MHD Equations

Necdet Aslan* and Terry Kammash†

*Fen-Ed. Physics Department, Marmara University, 81040 Göztepe İstanbul, Turkey; and †Nuclear Engineering Department, University of Michigan, Ann Arbor, Michigan 48109
E-mail: necdet@nem.nukleer.gov.tr

Received February 15, 1996; revised December 9, 1996

In this paper, the solution of a generalized system of hyperbolic equations by means of upwind, limited, second-order accurate fluxes including a new sonic fix is presented. The new sonic fix introduced here utilizes a dissipation term embedded directly in the fluxes and it is totally based on physical grounds producing the correct decay rate of sonic gradients. In addition to the sonic fix, the effects of the source term on the flux limiters are also introduced. The resulting scheme is applied to a variety of test problems resulting from the solutions of Euler's and magneto-hydrodynamic (MHD) equations. To eliminate the divergence problem, a new implementation of a recently introduced scheme for the MHD equations which includes a divergence wave and a source related to $\nabla \cdot \mathbf{B}$ is introduced. The numerical test results obtained with this new scheme are in excellent agreement with previous results and they show that the scheme presented here is robust, accurate, and entropy satisfying by producing very sharp contact discontinuities and shocks without postshock oscillations and divergence errors.

1. INTRODUCTION

The behavior of hyperbolic equations near sonic points is very critical. While algorithms including a reconstruction stage of primitive quantities are less affected by the sonic points, algorithms using flux limiters may lead to unphysical expansion shocks if the sonic points are not handled correctly. In this case the algorithm may not converge to the correct entropy satisfying solution. Treatments of sonic points have been developed so far by many investigators (see [1–4]). The most striking sonic fix was introduced recently by Roe [5] for the solutions of Euler's equations where both of the states around the sonic interfaces are modified to obtain the correct decay rate of sonic gradients. This idea was applied to the magnetohydrodynamic (MHD) equations by Aslan [6] and very satisfactory results were obtained with the requirement of no structure coefficients used in [7]. The new sonic fix introduced here follows an idea similar to that given in [5] but it differs in the sense that it is embedded directly in fluxes and that it requires no additional modification of the left and right states around the sonic interface as done in [5]. As in [4, 5], it relies on the physical grounds and it leads to the correct amount of sonic flux transfer between the related states, producing a correct decay rate of sonic gradients.

Section 2 describes the basic equations of generalized hyperbolic equations with source and a second-order accurate numerical scheme with a new sonic fix and a source parameter. An appropriate flux limiter which includes the effects of the source and sonic fix parameters is found and a modified Superbee limiter is introduced in Section 3. It is shown that the lower and upper bounds of the limiter should be modified when the source parameter is significantly greater than unity. In Section 4, the conservative form of ideal MHD equations and the parameters required for the new sonic fix are given. Secton 5 gives one- and two-dimensional numerical results to show the excellent performance of the new sonic fix and the new divergence source along with the divergence wave. Finally, the conclusion is given in Section 6.

2. BASIC EQUATIONS

The nonconservative form of the system of hyperbolic partial differential equations in one space dimension is

$$\mathbf{u}_t + A(\mathbf{u})\mathbf{u}_x = \mathbf{s}, \tag{1}$$

where $\mathbf{u}(x, t)$ is the m component state vector and $\mathbf{s}(x, t)$ is the source vector. The conservative form of (1) with the flux function $\mathbf{f}(\mathbf{u})$ that satisfies $A = \partial\mathbf{f}/\partial\mathbf{u}$ is given by

$$\mathbf{u}_t + \mathbf{f}(\mathbf{u})_x = \mathbf{s}. \tag{2}$$

The system given by (1) or (2) is hyperbolic if the $m \times m$ flux-to-state Jacobian matrix, A, is diagonalizable with real eigenvalues such that the following decomposition is allowed

$$A = R\Lambda R^{-1}, \tag{3}$$

0021-9991/97 $25.00

where Λ is the diagonal matrix of eigenvalues and $R = [\mathbf{r}_1|\mathbf{r}_2\cdots|\mathbf{r}_m]$ is the column matrix of m right eigenvectors. This eigenvalue equation can be written in component form as

$$A\mathbf{r}_k = \lambda_k \mathbf{r}_k, \quad k = 1, 2, ..., m, \tag{4}$$

where now $\mathbf{r}_k$ is defined as the right eigenvector of kth eigenvalue, λ_k. If the Jacobian matrix is constant, the equation set is linear and the flux satisfies $\mathbf{f} = A\mathbf{u}$; therefore (1) trivially leads to (2). The nonlinearity in the system, arising from the Jacobian varying with $\mathbf{u}$, can be removed by linearizing it with a Jacobian frozen at $\tilde{A} = A(\tilde{u})$. The required average state, $\tilde{\mathbf{u}}$, for converting (1) into (2) systematically can be found from the identity $\mathbf{f}_x = \tilde{A}\mathbf{u}_x$ (called the Rankine–Hugoniot, R–H, relations).

The initial input, $\mathbf{u}(x, 0)$, for the above system of equations is usually chosen such that the state denotes the cell averages that are piecewise continuous. In this case, at each cell edge there is a discontinuity (unless the state is constant) and one must solve a Riemann problem locally. Since the Riemann solution represents a wavelike character, such a discontinuity located at, say x_0, will give rise to the production of m different families of waves propagating with a speed λ_k along the curves $x = x_0 + \lambda_k t$ (characteristics) on the x–t plane. In this case, the solution (which can be viewed as being the superposition of m waves, each of which is advected independently) can be found along these characteristic curves. These curves are straight lines if the Jacobian matrix is constant at all times; otherwise, each characteristic speed depends on the solution itself, and the problem becomes nonlinear. This difficulty can be overcome by linearizing the system around an average state $\tilde{\mathbf{u}}^n$ from which the characteristics are found and then the solution at t^{n+1} is obtained.

Now discretize the x–t plane by choosing an appropriate mesh of width Δx and time step of Δt and let $x_{i\pm1/2} = (i \pm 1/2)\,\Delta x$ be the boundary locations of cell i, and let $t^n = n\,\Delta t$, $n = 0, 1, 2, ...$, be the time level which is restricted by the Courant–Friedrichs–Lewy condition. In the finite-volume method, (2) is integrated over the finite volume of the cell (*i.e.,* here the finite area on the x–t plane) and converted into the following integral form,

$$\begin{aligned}\int_{x_{i-1/2}}^{x_{i+1/2}} [\mathbf{u}(x, t^{n+1}) - \mathbf{u}(x, t^n)]\,dx \\ = -\int_{t^n}^{t^{n+1}} [\mathbf{f}(x_{i+1/2}, t) - \mathbf{f}(x_{i-1/2}, t)]\,dt \\ + \int_{i_{i-1/2}}^{x_{i+1/2}} \int_{t^n}^{t^{n+1}} \mathbf{s}(x, t)\,dx\,dt,\end{aligned} \tag{5}$$

which yields important shock capturing properties and gives rise to the following definitions of cell-averaged state, source, and the numerical flux respectively,

$$\mathbf{U}_i^n = \frac{1}{\Delta x}\int_{i_{i-1/2}}^{x_{i+1/2}} \mathbf{u}(x, t^n)\,dx, \tag{6}$$

$$\mathbf{S}_i^{n+1/2} = \frac{1}{\Delta x\,\Delta t}\int_{x_{i-1/2}}^{x_{i+1/2}}\int_{t^n}^{t^{n+1}} \mathbf{s}(x, t)\,dx\,dt, \tag{7}$$

$$\mathbf{F}_{i\pm1/2}^{n+1/2} = \frac{1}{\Delta t}\int_{t^n}^{t^{n+1}} \mathbf{f}(x_{i\pm1/2}, t)\,dt. \tag{8}$$

Employing these in (5) leads to the more familiar scheme

$$\mathbf{U}_i^{n+1} = \mathbf{U}_i^n - \frac{\Delta t}{\Delta x}[\mathbf{F}_{i+1/2}^{n+1/2} - \mathbf{F}_{i-1/2}^{n+1/2}] + \Delta t\mathbf{S}_i^{n+1/2}. \tag{9}$$

Note that if $\mathbf{F}_{i+1/2}$ increases the state in cell $i + 1$, the same amount is decreased in cell i. Thus the form given by (9) guarantees that the physical quantities (mass, momentum, current, etc.) are affected by the flows into or out of the first and last cells (telescoping property) and by the source within the domain. The sources may arise in hyperbolic differential equations due to the actual external forces, the coordinate curvature, the divergence condition, etc. Regardless of the fact that the existence of the sources will affect the solution and hence the shock structure, one still must integrate the homogeneous part of the equations in conservative form. In this paper, the effect of the source vector is included in the fluxes by projecting it onto the right eigenvectors so that its effect will advect correctly in the medium. As an example, the correct advection of the divergence wave in MHD can only be ensured by considering an eight-wave eigensystem and a small-magnitude source vector related to $\nabla \cdot \mathbf{B}$. Projecting the source vector onto the eigenvectors was first introduced by Glaister [8], who investigated the spherical shock reflection from the origin and obtained much better results than those of Noh [9]. This procedure was also outlined and explained by Roe [10]. Recently, having produced comparable results, Aslan [6] examined this technique and explained the effect of the source term and the underlying physics about the origin heating in spherical geometry. Implementing these ideas into the MHD and modifying the fluxes bring about new limitations on the flux limiters. Thus, in what follows a formal presentation of how the flux limiters should be obtained is given in detail.

Provided that the flux and source vectors in (9) are calculated such that the conservation is maintained, this scheme can be used to update $\mathbf{U}_i^n$ by an appropriate time marching procedure (explicit, implicit, Runga–Kutta, etc.). To obtain second-order accuracy in time in 1D problems,

the Lax–Wendroff (L–W) method based on the following Taylor's series can be used,

$$\mathbf{U}_i^{n+1} = \mathbf{U}_i^n + \Delta t(\mathbf{U}_t)_i + \frac{\Delta t^2}{2}(\mathbf{U}_{tt})_i + O(\Delta t^3), \qquad (10)$$

whose last two terms before truncation can be written from (2) as

$$\begin{aligned}\mathbf{U}_t &= \mathbf{S} - \mathbf{F}_x\\ \mathbf{U}_{tt} &= \mathbf{S}_t - A_t\mathbf{U}_x - A(\mathbf{S} - \mathbf{F}_x)_x\\ &= \mathbf{S}_t - (A\mathbf{S})_x + A_x\mathbf{F}_x + A(\mathbf{F}_x)_x\\ &= \mathbf{S}_t - (A\mathbf{S})_x + (A\mathbf{F}_x)_x\end{aligned}$$

using $\mathbf{F}_x = A\mathbf{U}_x$ and $A_t\mathbf{U}_x = A_u\mathbf{U}_t\mathbf{U}_x = A_x\mathbf{U}_t$. Note that the same form for $\mathbf{U}_{tt}$ could have been obtained in fewer steps if $\mathbf{F}_{xt} = (\mathbf{F}_t)_x = (A\mathbf{U}_t)_x$ was used. The reason for writing $\mathbf{U}_{tt}$ in this form is to put it in terms of $A_x\mathbf{F}_x$ which acts as a dissipation term that is maximized only at sonic points. This is clear for scalar problems since $a \approx 0$, $a_x \to$ max defines a local sonic point. For the systems of equations, the vector $A_x\mathbf{F}_x$ will have a local maximum at a sonic point associated with the kth eigenvalue that satisfies $\lambda_L < 0$, $\lambda_R > 0$, $\lambda_{i+1/2} \approx 0$. Thus the term $A_x\mathbf{F}_x$ seems to be a good candidate for this purpose, and it can be used pointwise to produce an additional dissipation for the sonic flux at the sonic points. The physical effect of this term can be described as follows:

Assume that the interface at $x_{i+1/2}$ includes a sonic point and hence a sonic flux, $F^*_{i+1/2}$. Then the updates of the states on both sides of this interface will be given by

$$U_i^{n+1} = U_i^n - \frac{\Delta t}{\Delta x}[F^*_{i+1/2} - F_{i-1/2}] \qquad (11)$$

$$U_{i+1}^{n+1} = U_{i+1}^n - \frac{\Delta t}{\Delta x}[F_{i+3/2} - F^*_{i-1/2}], \qquad (12)$$

neglecting the source terms. Writing the first-order part of the sonic flux as (see Eq.(29))

$$\begin{aligned}F^*_{i+1/2} &= (1 - \mathscr{K}^*)\frac{F_i + F_{i+1}}{2} + \text{small terms}\\ &\approx \frac{F_i + F_{i+1}}{2} - \mathscr{K}^*F(\tilde{U}_{i+1/2}),\end{aligned} \qquad (13)$$

one sees that a contribution term $(\Delta t/\Delta x)\mathscr{K}^*F(\tilde{U})$ is transferred from U_{i+1} to U_i. To understand the physical significance underlying this transfer consider, for example, the x component of the momentum equation for MHD. After straightforward algebra one sees that this transferred quantity from the right momentum to the left one across the sonic interface is given by (these will be explained later in detail)

$$\begin{aligned}&\frac{\Delta t^2}{2\,\Delta x^2}(3 - \gamma)\left(\tilde{P} + \frac{\tilde{B}_y^2 + \tilde{B}_z^2}{8\pi} - \frac{\tilde{B}_x^2}{8\pi}\right)\\ &\qquad \Delta V_x + \text{small terms}.\end{aligned} \qquad (14)$$

This second-order contribution is related to the total perpendicular pressure and to the change in V_x (which has a local maximum at unphysical expansion shocks). This sonic transfer (as far as it is applied at only sonic points) reduces ΔV_x to the required levels as the iterations proceed and its effect becomes insignificant after the unphysical expansion shock is totally eliminated.

The numerous numerical results (some of which will be presented later) prove that adding this term into the fluxes at sonic points successfully eliminates the unphysical expansion shocks. The original feature in this new pointwise fix is that it is embedded automatically in the fluxes to transfer the right amount of flux between the cells around the sonic interface without the need of an extra modification of the scheme. Taking this extra term into consideration, (10) can be written to second order in time as

$$\begin{aligned}\mathbf{U}_i^{n+1} = \mathbf{U}_i^n + \Delta t(\mathbf{S} - \mathbf{F}_x)_i + \frac{\Delta t^2}{2}[&\mathbf{S}_t + (A\mathbf{F}_x)_x\\ &+ A_x^*\mathbf{F}_x - (A\mathbf{S})_x]_i,\end{aligned} \qquad (15)$$

where the term $A_x^*\mathbf{F}_x$ denotes the term to be applied pointwise at only sonic points. Rearranging this equation one gets

$$\begin{aligned}\mathbf{U}_i^{n+1} = \mathbf{U}_i^n - \Delta t(I - \mathscr{K}^*)[\mathbf{F}_x]_i + \frac{\Delta t^2}{2}[(A\mathbf{F}_x)_x - (A\mathbf{S})_x]_i\\ + \Delta t\mathbf{S}_i^n + \frac{\Delta t^2}{2}\left(\frac{\mathbf{S}_i^{n+1} - \mathbf{S}_i^n}{\Delta t}\right),\end{aligned} \qquad (16)$$

where I is the unit matrix and $\mathscr{K}^* \equiv (\Delta t/2)(A_{iti} - A_i)/\Delta x$ is called, here, the sonic fix matrix.

Defining $\mathscr{V} = (\Delta t/\Delta x)A$ as the local Courant matrix and $\mathbf{S}_i^{n+1/2} = (\mathbf{S}_i^{n+1} + \mathbf{S}_i^n)/2$ as the time-averaged source, the space derivatives in (16) are taken to second order and the following numerical scheme overall second-order accurate in both space and time (in 1D) is obtained:

$$\begin{aligned}\mathbf{U}_i^{n+1} = \mathbf{U}_i^n - \frac{\Delta t}{\Delta x}&\left[\begin{array}{c}(I - \mathscr{K}^*)\dfrac{\mathbf{F}_{i+1} - \mathbf{F}_{i-1}}{2} - \dfrac{\mathscr{V}_{i+1/2}}{2}(\mathbf{F}_{i+1} - \mathbf{F}_i)\\ + \dfrac{\mathscr{V}_{i-1/2}}{2}(\mathbf{F}_i - \mathbf{F}_{i-1}) + \dfrac{\Delta t}{2}(A_{i+1/2}\mathbf{S}_{i+1/2} - A_{i-1/2}\mathbf{S}_{i-1/2})\end{array}\right]\\ &+ \Delta t\,\mathbf{S}_i^{n+1/2}.\end{aligned} \qquad (17)$$

It is well known that upwind schemes produce better results near discontinuities and shocks, due to the fact that they utilize the information the characteristics carry to detect the correct direction of wave propagation. Conservative L–W fluxes, $\mathbf{F}^{\mathrm{LW}}$, that work well in smooth regions can be obtained easily from the terms in brackets in (17). With a simple modification, these fluxes can be written as a first-order upwind flux (which is monotonicity preserving but too much diffusive) plus an antidiffusive correction whose magnitude is to be limited by a limiter function $\Phi(\theta)$ depending on the smoothness of data

$$\mathbf{F}^{\mathrm{LW}} = \mathbf{F}^{1O} + [\mathbf{F}^{\mathrm{LW}} - \mathbf{F}^{1O}]\Phi(\theta), \tag{18}$$

where θ is defined as the ratio of the upwind flux to the interface flux (see Eq. (52)).

To introduce this idea, rewrite (17) in a form that includes an upwind, first-order flux plus an antidiffusive, limited correction in the following two different forms:

$$\begin{aligned}\mathbf{U}_i^{n+1} = \mathbf{U}_i^n &- \frac{\Delta t}{\Delta x}(I - \mathscr{K}^*)[\mathbf{F}_i - \mathbf{F}_{i-1}] + \Delta t \mathbf{S}_i^{n+1/2} \\ &- \frac{\Delta t}{\Delta x}\left[\frac{\Delta t}{2} A_{i+1/2}\mathbf{S}_{i+1/2}\right. \\ &\left. - \frac{1}{2}[\mathscr{V} - (I - \mathscr{K}^*)]_{i+1/2}(\mathbf{F}_{i+1} - \mathbf{F}_i)\right]\Phi_{i+1/2} \\ &\frac{\Delta t}{\Delta x}\left[\frac{\Delta t}{2} A_{i-1/2}\mathbf{S}_{i-1/2}\right. \\ &\left. - \frac{1}{2}[\mathscr{V} - (I - \mathscr{K}^*)]_{i-1/2}(\mathbf{F}_i - \mathbf{F}_{i-1})\right]\Phi_{i-1/2}\end{aligned} \tag{19}$$

$$\begin{aligned}\mathbf{U}_i^{n+1} = \mathbf{U}_i^n &- \frac{\Delta t}{\Delta x}(I - \mathscr{K}^*)[\mathbf{F}_{i+1} - \mathbf{F}_i] + \Delta t \mathbf{S}_i^{n+1/2} \\ &- \frac{\Delta t}{\Delta x}\left[\frac{\Delta t}{2} A_{i+1/2}\mathbf{S}_{i+1/2}\right. \\ &\left. - \frac{1}{2}[\mathscr{V} + (I - \mathscr{K}^*)]_{i+1/2}(\mathbf{F}_{i+1} - \mathbf{F}_i)\right]\Phi_{i+1/2} \\ &+ \frac{\Delta t}{\Delta x}\left[\frac{\Delta t}{2} A_{i-1/2}\mathbf{S}_{i-1/2}\right. \\ &\left. - \frac{1}{2}[\mathscr{V} + (I - \mathscr{K}^*)]_{i-1/2}(\mathbf{F}_i - \mathbf{F}_{i-1})\right]\Phi_{i-1/2}\end{aligned} \tag{20}$$

To maintain the upwinding property, the form given by (19) should be used when the characteristic speeds are always positive (i.e., $A > 0$) and (20) for $A < 0$. In this case, the first-order flux at the interface $i + 1/2$ will be $\mathbf{F}_i$ for $A > 0$ and $\mathbf{F}_{i+1}$ for $A < 0$. This leads to the following form valid for both directions of the flow [11]:

$$\mathbf{F}_{i+1/2}^{1O} = \frac{\mathbf{F}_i + \mathbf{F}_{i+1}}{2} - \frac{1}{2}\,\mathrm{sgn}(A)(\mathbf{F}_{i+1} - \mathbf{F}_i). \tag{21}$$

Since $\mathbf{F}_{i+1} - \mathbf{F}_i = \tilde{A}_{i+1/2}(\mathbf{U}_{i+1} - \mathbf{U}_i)$ from the R–H conditions and $\mathrm{sgn}(A)A = |A|$, the first-order fluxes become

$$F_{i\pm1/2}^{1O} = \frac{\mathbf{F}_i + \mathbf{F}_{i\pm1}}{2} \mp \frac{1}{2}|\tilde{A}_{i\pm1/2}|\,(\mathbf{U}_{i\pm1} - \mathbf{U}_i). \tag{22}$$

Combining the rest of the terms in (19) and (20) by means of σ, the sign of A, one gets the following upwind, second-order, limited interface fluxes in 1D

$$\begin{aligned}\mathbf{F}_{i+1/2} = (I - \mathscr{K}^*)&\left[\frac{\mathbf{F}_i + \mathbf{F}_{i\pm1}}{2} \mp \frac{1}{2}|\tilde{A}_{i\pm1/2}|(\mathbf{U}_{i\pm1} - \mathbf{U}_i)\right] \\ &\mp \frac{1}{2}\left[[\mathscr{V} - \sigma(I - \mathscr{K}^*)]\tilde{A}_{i\pm1/2}(\mathbf{U}_{i\pm1} - \mathbf{U}_i)\right. \\ &\left. \mp \frac{\Delta t}{2}(\tilde{A}\tilde{\mathbf{S}})_{i\pm1/2}\right]\Phi_{i\pm1/2}(\theta)\end{aligned} \tag{23}$$

to be used along with (9). Using (3), the discrete form of the R–H relations at the interfaces $i \pm 1/2$ becomes

$$\mathbf{F}_{i\pm1} - \mathbf{F}_i = \tilde{A}_{i\pm1/2}(\mathbf{U}_{i\pm1} - \mathbf{U}_i) = (\tilde{R}\tilde{\Lambda}\tilde{R}^{-1})_{i\pm1/2}(\mathbf{U}_{i\pm1} - \mathbf{U}_i). \tag{24}$$

Defining $(\alpha_k)_{i\pm1/2} = \pm(\mathbf{r}_k)^{-1}_{i\pm1/2}(\mathbf{U}_{i\pm1} - \mathbf{U}_i)$ as the strength of the kth wave, the relation

$$\pm(\mathbf{U}_{i\pm1} - \mathbf{U}_i) = \sum_k (\tilde{\alpha}_k\tilde{\mathbf{r}}_k)_{i\pm1/2} \tag{25}$$

will hold for the state differences so that (24) will lead to the relation

$$\pm(\mathbf{F}_{i\pm1} - \mathbf{F}_i) = \sum_k (\tilde{\lambda}_k\tilde{\alpha}_k\tilde{\mathbf{r}}_k)_{i\pm1/2} \tag{26}$$

for the flux differences. Since the source terms appearing in the second-order fluxes include the Jacobian matrices, they can also be projected onto the right eigenvectors as [8]

$$A_{i\pm1/2}\mathbf{S}_{i\pm1/2} = (\tilde{R}\tilde{\Lambda}\tilde{R}^{-1})_{i\pm1/2}\mathbf{S}_{i\pm1/2} = \sum_k (\tilde{\lambda}_k\tilde{\beta}_k\tilde{\mathbf{r}}_k)_{i\pm1/2}, \tag{27}$$

where here $\tilde{\beta}_k$ is called the strength of the source carried along with the kth wave. This lets

$$\mathbf{S}_{i\pm1/2} = \sum_k (\tilde{\beta}_k \tilde{\mathbf{r}}_k)_{i\pm1/2}. \tag{28}$$

Here $\tilde{\lambda}_k$ and $\tilde{\mathbf{r}}_k$ are the kth eigenvalue and right eigenvector of $\tilde{A}$ evaluated at the interfaces by means of the average state. Being an important part of the construction, this average state is found analytically by solving (25) and (26) simultaneously using the states on both sides of the interfaces which are the only available data. This usually requires straightforward but lengthy analytical derivations to be used by the numerical code (for an example see [12] for MHD). Thus, with these definitions, the second-order, upwind, limited interface fluxes become

$$\begin{aligned}\mathbf{F}_{i\pm1/2} = (I - \mathscr{K}^*)\frac{\mathbf{F}_i + \mathbf{F}_{i\pm1}}{2} - \frac{1}{2}\sum_k [(1-\kappa^*)|\tilde{\lambda}_k|\tilde{\alpha}_k\tilde{\mathbf{r}}_k]_{i\pm1/2} \\ \mp \frac{1}{2}\sum_k [\tilde{\lambda}_k((\tilde{\nu}_k - \tilde{\sigma}_k(1-\kappa^*))\tilde{\alpha}_k \\ \mp \Delta t\tilde{\beta}_k)\tilde{\mathbf{r}}_k]_{i\pm1/2}\Phi_{i\pm1/2}(\theta_u),\end{aligned} \tag{29}$$

where θ_u will be explained later. Here, $\tilde{\nu} = (\Delta t/\Delta x)\tilde{\lambda}$ is the local Courant number (which is to be held smaller than unity so that the waves from adjacent Riemann problems do not interact), $\tilde{\sigma}$ is the sign of $\tilde{\lambda}$, and $\kappa^*_{i\pm1/2} = \pm\frac{1}{2}(\Delta t/\Delta x)(\tilde{\lambda}_{i\pm1} - \tilde{\lambda}_i) = \pm\frac{1}{2}(\tilde{\nu}_{i\pm1} - \tilde{\nu}_i)$ is called the sonic fix parameter and is applied only at sonic points.

Many investigators tried to design methods to smooth the solutions near sonic points by introducing a small dissipation. The main idea of some of these fixes was to replace $|\lambda_k|$ in (29) with a smooth function near the sonic point. Harten *et al.* replaced $|\lambda_k|$ with

$$|\lambda_k| = \begin{cases} |\lambda_k|, & \text{if } |\lambda_k| \geq \varepsilon \\ \dfrac{1}{2}\left(\dfrac{\lambda_k^2 + \varepsilon^2}{\varepsilon}\right), & \text{otherwise,} \end{cases} \tag{30}$$

where ε is a small number. van Leer *et al.* [3] treated each wave differently and used

$$|\lambda_k| = \begin{cases} |\lambda_k| & \text{if } |\lambda_k| \geq \dfrac{1}{2}\delta\lambda_k \\ \dfrac{\lambda_k^2}{\delta\lambda_k} + \dfrac{1}{4}\delta\lambda_k & \text{if } |\lambda_k| < \dfrac{1}{2}\delta\lambda_k \end{cases} \tag{31}$$

$$\delta\lambda_k = \max(4\Delta\lambda_k, 0), \quad \Delta\lambda_k = \lambda_{i+1}^k - \lambda_i^k.$$

LeVeque [4] replaced the flux, $F_{i+1/2}$, in (29) by

$$F_{i+1/2} = \frac{1}{2}(F_i + F_{i+1}) - \frac{1}{2}\sum_k \tilde{\alpha}_k[\hat{\lambda}^*_{kr} - \hat{\lambda}^*_{kl}]\tilde{\mathbf{r}}_k, \tag{32}$$

where he used

$$\hat{\lambda}^*_{kr} = \lambda^{R+}\left(\frac{\tilde{\lambda}_{i+1/2} - \lambda^{R-}}{\lambda^{R+} - \lambda^{R-}}\right), \quad \hat{\lambda}^*_{kl} = \lambda^{L-}\left(\frac{\lambda^{R+} - \tilde{\lambda}_{i+1/2}}{\lambda^{R+} - \lambda^{R-}}\right) \tag{33}$$

$$\lambda^{R+} = \max(\lambda_{i+1}, 0), \qquad \lambda^{L-} = \min(\lambda_i, 0). \tag{34}$$

Roe [5] differentiated (1) with respect to x and obtained $l\cdot[\mathbf{u}_{xt} + A_x\mathbf{u}_x] = 0$ for the sonic points (at which $A = 0$), where he defined $l\cdot\mathbf{u}_{xt}$ as a measure at which the sonic field is decaying. He suggested that a term $(\kappa\cdot\mathbf{r})_{i+1/2}$, where $\kappa \equiv \frac{1}{2}l\cdot[\mathbf{u}_{xt}\,\Delta x\,\Delta t - (\delta\mathbf{u}_{i+1} - \delta\mathbf{u}_i)]$ (with $\delta\mathbf{u}_i = \mathbf{u}_i^{n+1} - \mathbf{u}_i^n$) should be transferred from $\mathbf{u}_{i+1}^{n+1}$ to $\mathbf{u}_i^{n+1}$ to correct them around the sonic interface. Compared with the sonic fixes given in [1–3], the new sonic fix introduced in this paper differs in the sense that it relies on physical grounds and it is embedded in the sonic flux directly (as done by LeVeque [4]). The new sonic fix and Roe's fix originate from a careful examination of (10) near sonic points. While Roe corrects the states after an intermediate solution is obtained, the new sonic fix described here is embedded into the fluxes so that the sonic points are handled automatically. As will be shown by numerical results, the new sonic fix successfully handles the sonic points, eliminating unphysical expansion shocks.

The classical L–W scheme works well for smooth regions but it produces spurious oscillations near discontinuities even though the first-order scheme does not. For this reason, the second-order antidiffusive flux may need to be adjusted near discontinuities. This suggests that the flux limiter should be a function of θ, the consecutive gradients of state, or flux differences. How this is done and what the lower and upper limits of this function should be are all explained in the next section in detail.

3. FLUX LIMITERS

While advancing the solution in time, it is desired that the monotonicity in the solutions be preserved in order to not get spurious oscillations near the discontinuities. It was seen earlier that the average state, $\tilde{\mathbf{U}}_{i+1/2}$, evaluated at the interface $i + 1/2$ is an important part of the construction of the scheme. If it is desirable to keep this state, which is an average of the states $\mathbf{U}_i$ and $\mathbf{U}_{i+1}$, monotonic, both of these states should be kept monotonic simultaneously. The monotonicity can be explained by means of the total variation of the solution at the new time level (i.e., $TV(\mathbf{U}^{n+1}) = \sum_i |\mathbf{U}_{i+1}^{n+1} - \mathbf{U}_i^{n+1}|$; see [13] for detailed explanations on the concepts of monotonicity, total variation stability, etc.).

The numerical scheme is said to be total variation diminishing (TVD) and monotonicity preserving if the relation

$$TV(\mathbf{U}^{n+1}) \leq TV(\mathbf{U}^n) \tag{35}$$

is satisfied for all n. For a general numerical scheme written in the form

$$\mathbf{U}_i^{n+1} = \mathbf{U}_i^n - C_{i-1/2}(\mathbf{U}_i^n - \mathbf{U}_{i-1}^n) + D_{i+1/2}(\mathbf{U}_{i+1}^n - \mathbf{U}_i^n), \quad (36)$$

it is easily shown that sufficient conditions for it to be TVD are given by the following inequalities [13]:

$$C_{i-1/2}, D_{i+1/2} \geq 0, \quad C_{i-1/2} + D_{i+1/2} \leq 1. \quad (37)$$

Considering the interface $i + 1/2$, it is clear that the state $\mathbf{U}_i$ carries the information if the flow is in the $+x$ direction and $\mathbf{U}_{i+1}$ when the flow is in the reverse direction. Thus, in order to preserve monotonicity in $\tilde{\mathbf{U}}_{i+1/2}$, $\mathbf{U}_i$ is to be limited for $A > 0$ and $\mathbf{U}_{i+1}$ for $A < 0$. This suggests that the form (19) should be used to limit $\mathbf{U}_i$ with $\tilde{A} > 0$ and (20) to limit $\mathbf{U}_{i+1}$ with $\tilde{A} < 0$. Implementing the R–H relations, (19) can be written without the last source term as

$$\mathbf{U}_i^{n+1} = \mathbf{U}_i^n - \frac{\Delta t}{\Delta x}\Big[(I - \mathscr{K}^*)A_{i-1/2}(\mathbf{U}_i - \mathbf{U}_{i-1}) + (\mathbf{F}^+_{i+1/2}\Phi_{i+1/2} - \mathbf{F}^+_{i-1/2}\Phi_{i-1/2})\Big], \quad (38)$$

where

$$\mathbf{F}^+_{i\pm1/2} = \frac{1}{2}\,\mathscr{V}_{i+1/2}[\Delta t\mathbf{S}_{i\pm1/2} \pm (I - \mathscr{K}^* - \mathscr{V})_{i+1/2}(\mathbf{U}_{i\pm1} - \mathbf{U}_i)] \quad (39)$$

are defined as unlimited second-order L–W fluxes. Factoring $\mathbf{F}^+_{i-1/2}$ and rearranging, (38) turns into

$$\mathbf{U}_i^{n+1} = \mathbf{U}_i^n - \frac{\Delta t}{\Delta x}\Big[(I - \mathscr{K}^*)A_{i-1/2} + \left[\frac{A}{2}(I - \mathscr{K}^* - \mathscr{V} + \omega)\right]_{i-1/2}\left(\frac{\Phi_{i+1/2}}{\theta^+} - \Phi_{i-1/2}\right)\Big](\mathbf{U}_i - \mathbf{U}_{i-1}), \quad (40)$$

where

$$\theta^+ = \frac{\mathbf{F}^+_{i-1/2}}{\mathbf{F}^+_{i+1/2}} = \frac{(A_{i-1/2}/2)(I - \mathscr{K}^* - \mathscr{V} + \omega)_{i-1/2}(\mathbf{U}_i - \mathbf{U}_{i-1})}{(A_{i+1/2}/2)(I - \mathscr{K}^* - \mathscr{V} + \omega)_{i+1/2}(\mathbf{U}_{i+1} - \mathbf{U}_i)} \quad (41)$$

and $\omega \equiv \Delta t\mathbf{S}/\Delta\mathbf{U}$ is defined as the source parameter here. Considering (36), the equation above leads to $D_{i+1/2} = 0$ and

$$C_{i-1/2} = (1 - \mathscr{K}^*)\,\mathscr{V}_{i-1/2} + \left[\frac{\mathscr{V}}{2}(1 - \mathscr{K}^* - \mathscr{V} + \omega)\right]_{i-1/2}\left[\frac{\Phi_{i+1/2}}{\theta^+} - \Phi_{i-1/2}\right]. \quad (42)$$

For the flow with $\tilde{A} < 0$, the form (20) is written for $\mathbf{U}_{i+1}$ as

$$\mathbf{U}_{i+1}^{n+1} = \mathbf{U}_{i+1}^n - \frac{\Delta t}{\Delta x}\Big[-(I - \mathscr{K}^*)\,\mathscr{V}_{i+3/2}(\mathbf{U}_{i+2} - \mathbf{U}_{i+1}) + (\mathbf{F}^-_{i+3/2}\Phi_{i+3/2} - \mathbf{F}^-_{i+1/2}\Phi_{i+1/2})\Big], \quad (43)$$

where

$$\mathbf{F}^-_{i+3/2} = \frac{A_{i+3/2}}{2}\,\omega - (I - \mathscr{K}^* - \mathscr{V})_{i+3/2}(\mathbf{U}_{i+2} - \mathbf{U}_{i+1}). \quad (44)$$

Modifying, one gets

$$\mathbf{U}_{i+1}^{n+1} = \mathbf{U}_{i+1}^n - \left[(I - \mathscr{K}^*)\,\mathscr{V}_{i+3/2} + \left[\frac{\mathscr{V}}{2}(I - \mathscr{K}^* - \mathscr{V} + \omega)\right]_{i+3/2}\left(\frac{\Phi_{i+1/2}}{\theta^-} - \Phi_{i+3/2}\right)\right](\mathbf{U}_{i+2} - \mathbf{U}_{i+1}), \quad (45)$$

where

$$\theta^- = \frac{\mathbf{F}^-_{i+3/2}}{\mathbf{F}^-_{i+1/2}} = \frac{(A_{i+3/2}/2)(I - \mathscr{K}^* + \mathscr{V} - \omega)_{i+3/2}(\mathbf{U}_{i+2} - \mathbf{U}_{i+1})}{(A_{i+1/2}/2)(I - \mathscr{K}^* + \mathscr{V} - \omega)_{i+1/2}(\mathbf{U}_{i+1} - \mathbf{U}_i)}. \quad (46)$$

With a similar consideration of (36), this form leads to $C_{i+1/2} = 0$ and

$$D_{i+3/2} = -(1 - \mathscr{K}^*)\,\mathscr{V}_{i+3/2} - \frac{\mathscr{V}_{i+3/2}}{2}(1 - \mathscr{K}^* + \mathscr{V} - \omega)_{i+3/2}\left[\frac{\Phi_{i+1/2}}{\theta^-} - \phi_{i+3/2}\right]. \quad (47)$$

Therefore, in order to preserve the monotonicity in the average state, $\mathbf{U}_{i+1/2}$, $C_{i-1/2}$ given by (42) and $D_{i+3/2}$ given

by (47) should be bound by the following inequalities respectively

$$0 \le (1 - \mathscr{K}^*)\,\mathscr{V}_{i-1/2} + \left[\frac{\mathscr{V}}{2}(1 - \mathscr{K}^* - \mathscr{V} + \omega)\right]_{i-1/2} \left[\frac{\phi_{i+1/2}}{\theta^+} - \Phi_{i-1/2}\right] \le 1, \quad A > 0 \tag{48}$$

$$0 \le -(1 - \mathscr{K}^*)\,\mathscr{V}_{i+3/2} - \left[\frac{\mathscr{V}}{2}(1 - \mathscr{K}^* + \mathscr{V} - \omega)\right]_{i+3/2} \left[\frac{\Phi_{i+1/2}}{\theta^-} - \Phi_{i+3/2}\right] \le 1, \quad A < 0. \tag{49}$$

Both of these can be combined to get an inequality that holds for both directions,

$$0 \le (1 - \mathscr{K}^*)|\mathscr{V}_u| + \frac{|\mathscr{V}_u|}{2}(1 - \mathscr{K}^* - |\mathscr{V}_u| + \sigma\omega_u) \left[\frac{\Phi_{i+1/2}}{\theta_u} - \Phi_u\right] \le 1, \tag{50}$$

or modifying one gets

$$-2\frac{(1 - \mathscr{K}^*)}{1 - \mathscr{K}^* - |\mathscr{V}_u| + \sigma\omega_u} \le \left[\frac{\Phi_{i+1/2}}{\theta_u} - \Phi_u\right] \le 2\frac{1/|\mathscr{V}_u| - (1 - \mathscr{K}^*)}{1 - \mathscr{K}^* - |\mathscr{V}_u| + \sigma\omega_u}, \tag{51}$$

where the subscript u denotes the upwind direction and should be taken as $i - 1/2$ for positive wave speeds ($A > 0$) and $i + 3/2$ for negative wave speeds ($A < 0$).

In this case, the limiter introduced in (29) should be a function of θ_u defined as

$$\tilde{\theta}_u^k = \frac{(1 - \sigma_k)\tilde{b}_{i+3/2}^k + (1 + \sigma_k)\tilde{b}_{i-1/2}^k}{2\tilde{b}_{i+1/2}^k}, \qquad \tilde{b}_{i+1/2}^k = \left[\frac{1}{2}(1 - \kappa^* - |\nu_k| + \sigma\omega)\tilde{\lambda}_k\tilde{\alpha}_k\tilde{\mathbf{r}}_k\right]_{i+1/2}. \tag{52}$$

It must be noted here that $\tilde{b}_{i\pm1/2}^k$ should be multiplied by $(\Delta t/\Delta x)_{i\pm1/2}$ whenever variable mesh is used. Therefore the inequality (51) leads to

$$0 \le \Phi(\theta) \le 2\frac{(1 - \mathscr{K}^*)}{1 - \mathscr{K}^* - |\mathscr{V}| + \sigma\omega}, \qquad 0 \le \frac{\Phi(\theta)}{\theta} \le 2\frac{1/|\mathscr{V}| - (1 - \mathscr{K}^*)}{1 - \mathscr{K}^* - |\mathscr{V}| + \sigma\omega}. \tag{53}$$

Since the effect of the sonic fix in the second-order part of the fluxes is negligible, this can be simplified to

$$0 \le \Phi(\theta) \le 2\frac{1}{1 - |\mathscr{V}|}, \quad 0 \le \frac{\Phi(\theta)}{\theta} \le \frac{2}{|\mathscr{V}|} \tag{54}$$

whenever $|\omega| \ll 1$. Furthermore, this set is often simplified with a safer set given by

$$0 \le \Phi(\theta) \le 2, \quad 0 \le \frac{\Phi(\theta)}{\theta} \le 2. \tag{55}$$

The above description shows that the limiters should include the source parameter, ω, when the source exists. It is recommended that the limiter be turned off whenever $|\omega| \gg 1$ since the bound for the limiter is lowered.

A wide variety of limiters have been introduced by investigators for different problems involving hyperbolic equations. Among these, the limiter (satisfying (54) and called Ultrabee [14]) that treats each wave differently is given by

$$\Phi^{\mathrm{u}}(\theta) = \max\left(0, \min\left(\frac{2\theta}{1 - |\nu|}, \max\left(1, \min\left(\theta, \frac{2}{|\nu|}\right)\right)\right)\right). \tag{56}$$

This limiter is rather compressive (i.e., produces very sharp discontinuities) but it leads to small postshock oscillations and wall heating in contact discontinuities. Another limiter, which treats the waves in an equal manner (satisfying (55)), called Superbee [14]), is given by

$$\Phi^{\mathrm{s}}(\theta) = \max(0, \min(2\theta, \max(1, \min(\theta, 2)))). \tag{57}$$

Like Ultrabee, this limiter preserves the transition widths of the discontinuities over many thousands of time steps but it slightly squares off maxima. The minmod limiter which produces less sharp diffusive shocks but very little postshock oscillations [14] is given by

$$\Phi^{\mathrm{m}}(\theta) = \max(0, \min(\theta, 1)). \tag{58}$$

van Leer's and van Albada's limiters produce diffusive shocks but behave well at maxima (i.e., $\theta < 0$):

$$\Phi^{\mathrm{vL}}(\theta) = \frac{|\theta| + \theta}{1 + |\theta|}, \quad \Phi^{\mathrm{vA}}(\theta) = \frac{2\theta^2 + \theta}{2\theta^2 - \theta + 2}. \tag{59}$$

We have experienced that if the Superbee limiter is modified as

$$\Phi^{\mathrm{ms}}(\theta) = \max(0, \min(2\theta, \max(1, \min(\theta, 2)))) + \min(0, \max(2\theta, \min(-1, \max(\theta, -2)))) \tag{60}$$

to include the case $\theta < 0$, it behaves very well at maxima. In this case, not only the discontinuities remain sharp but the maxima are not squared off as well.

As a concluding remark, we state that the numerical form given by (9) handles the sonic points well and solves the conservative form of the hyperbolic equations (2) successfully provided that the fluxes given by (29) include the new sonic fix and the limiter function defined by (60) as a function of θ given by (52).

4. MHD EQUATIONS

MHD is the simplest model that can describe the macroscopic behavior [6] of the plasma as a fluid. The model describes how external and/or internal fields as well as other forces can interact with plasma. With the MHD equations, not only astrophysical plasmas can be investigated but also the magnetic and electrical properties of different types of fusion reactors (such as tokamaks or spheromaks [15]) can be investigated. The ideal MHD equations in conservative form are given by

$$\frac{\partial}{\partial t}\begin{bmatrix}\rho\\ \rho\mathbf{v}\\ \mathbf{B}\\ E\end{bmatrix}+\boldsymbol{\nabla}\cdot\begin{bmatrix}\rho\mathbf{v}\\ \rho\mathbf{v}\mathbf{v}+I\left(P+\dfrac{\mathbf{B}\cdot\mathbf{B}}{8\pi}\right)-\dfrac{\mathbf{B}\mathbf{B}}{4\pi}\\ \mathbf{v}\mathbf{B}-\mathbf{B}\mathbf{v}\\ \left(E+P+\dfrac{\mathbf{B}\cdot\mathbf{B}}{8\pi}\right)\mathbf{v}-\dfrac{\mathbf{B}}{4\pi}(\mathbf{v}\cdot\mathbf{B})\end{bmatrix}=-\begin{bmatrix}0\\ \dfrac{\mathbf{B}}{4\pi}\\ \mathbf{v}\\ \dfrac{\mathbf{v}\cdot\mathbf{B}}{4\pi}\end{bmatrix}\boldsymbol{\nabla}\cdot\mathbf{B}, \tag{61}$$

here ρ is the density, $\mathbf{v}$ is the velocity, $\mathbf{B}$ is the magnetic field, P is the pressure, and $E = \rho V^2/2 + B^2/8\pi + P/(\gamma - 1)$ is the total energy with γ, the ratio of the specific heats.

Preserving $\boldsymbol{\nabla}\cdot\mathbf{B} = 0$ to the highest accuracy is very crucial for the discretized versions of the MHD equations. If this condition is not preserved the monopole forces along the direction of the magnetic field will be created and a nonphysical fluid dynamics will be produced (see Brackbill and Barnes [16]). The divergence condition in one-dimensional MHD equations reduces to $B_x = \text{const.}$, giving rise to a 7×7 eigensystem of the Jacobian with a vanishing divergence source. For two- or three-dimensional problems, instead of writing the seven-wave system and then cleaning up the divergence in a separate step, it is better to work with the eight-wave system which leads to a slightly nonconservative form due to the divergence source. In fact extra cleaning may be required for the problems with stagnation points or recirculation zones. The singularity related to $\boldsymbol{\nabla}\cdot\mathbf{B} = 0$ is eliminated by adding a divergence wave, resulting in a modified Jacobian with an 8×8 eigensystem and a source related to $\boldsymbol{\nabla}\cdot\mathbf{B}$. This idea was first introduced by Aslan [6], and first implemented in two dimensions by Powell [17] and Gombosi *et al.* [18].

The details of this modification and the eigensystem will not be given here but the first seven components of the sonic fix vector normal to the sonic interface (i.e., $\mathscr{K}^*F(\tilde{U}) \equiv (\Delta t/2)(\Delta A/\Delta x)\cdot\tilde{\mathbf{F}}$) which appears in (29) are introduced. The first seven components of this vector (without the factor of $\Delta t/2\,\Delta x$) are given by

$$\kappa_1, \kappa_5 = 0, \quad \kappa_2 = (3-\gamma)\left(\mathbf{P}_\perp^* - \frac{B_n^2}{8\pi}\right)\Delta V_n + \frac{\gamma-1}{4\pi}B_n(B_t\,\Delta V_t + \mathbf{B}_\perp\,\Delta V_\perp) \tag{62}$$

$$+\frac{2-\gamma}{4\pi}(V_nB_t - V_tB_n)\,\Delta B_t + \frac{2-\gamma}{4\pi}(V_nB_\perp - V_\perp B_n)\,\Delta B_\perp \tag{63}$$

$$\kappa_{3,4} = \left(P_\perp^* - \frac{B_n^2}{8\pi}\right)\Delta V_{t,z} - \frac{B_nB_t}{4\pi}\Delta V_n + \frac{V_tB_n - V_nB_t}{4\pi}\Delta B_n \tag{64}$$

$$\kappa_{6,7} = B_nV_n\,\Delta V_{t,z} - V_{t,z}B_n\,\Delta V_n + \left(P_\perp^* - \frac{B_n^2}{8\pi}\right)\Delta\left(\frac{B_{t,z}}{\rho}\right) + \frac{B_nB_{t,z}}{4\pi}\Delta\left(\frac{B_n}{\rho}\right), \tag{65}$$

where the indices t and n denote the tangential and normal directions to the sonic interface, Δ denotes the jump of the physical quantities across the sonic interface, and $P_\perp^* = P + (B_t^2 + B_z^2)/8\pi$ defines the total perpendicular pressure. Our experience shows that the first term in κ_2 is the most significant term in this new fix; and using only this term in κ_2 while taking other κ's zero leads to an extremely robust scheme producing rather satisfactory results.

When the differential form of the MHD equations is

integrated over the finite volume in two-dimensional Cartesian geometry with $\partial/\partial z = 0$, one gets

$$\int\int\int_V \mathbf{U}_t \, dA \, dt + \int\int\int_V [\mathbf{F}_x + \mathbf{G}_y] \, dA \, dt = \int\int\int_V \mathbf{S} \, dA \, dt. \tag{66}$$

Defining $\langle \mathbf{U}^n \rangle = (1/A) \int\int_A \mathbf{U}^n \, dA$ and $\langle \mathbf{S}^{n+1/2} \rangle = (1/A) \int\int_A \mathbf{S}^{n+1/2} \, dA$ as the average state and source vectors one gets the following form that can be used with quadrilateral cells,

$$\langle \mathbf{U}^{n+1} \rangle = \langle \mathbf{U}^n \rangle - \frac{\Delta t}{A} \sum_{k=1}^{4} (\mathbf{F}^{n+1/2} \, dy - \mathbf{G}^{n+1/2} \, dx) + \Delta t \langle \mathbf{S}^{n+1/2} \rangle \tag{67}$$

$$\langle \mathbf{U}_{i,j}^{n+1} \rangle = \langle \mathbf{U}_{i,j}^{n} \rangle - \frac{\Delta t}{A_{i,j}} \sum_{k=1}^{4} \mathbf{F}_n^k \cdot \Delta \mathbf{S}_k + \Delta t < \mathbf{S}_{i,j}^{n+1/2} \rangle, \tag{68}$$

where $A_{i,j}$ is the area of the cell, ΔS_k is the length of its kth side, and $\mathbf{F}_n$ is the normal flux across this cell face. The 2D algorithm is implemented as follows:

Because the source term at $t^{n+1/2}$ is unknown, (68) is split into two steps. First the update $\mathbf{U}^*$ is found from

$$\langle \mathbf{U}_{i,j}^{*} \rangle = \langle \mathbf{U}_{i,j}^{n} \rangle - \frac{\Delta t}{A_{i,j}} \sum_{k=1}^{4} \mathbf{F}_n^k \cdot \Delta S_k + \Delta t \langle \mathbf{S}_{i,j}^{n} \rangle \tag{69}$$

and from this update a new source term $\mathbf{S}_{i,j}^{*,n+1}$ is calculated which is used to correct the updated state

$$\langle \mathbf{U}_{i,j}^{n+1} \rangle = \langle \mathbf{U}_{i,j}^{*} \rangle + \frac{\Delta t}{2} [\mathbf{S}_{i,j}^{*,n+1} - \langle \mathbf{S}_{i,j}^{n} \rangle]. \tag{70}$$

The numerical tests showed that most of the time the correction step (70) has no significant effect. It is noted however that this correction may be important for stiff sources! One point that needs to be clarified is that since x and y fluxes are evaluated simultaneously at the predictor step (Eq. (69)) rather than in seperate steps (such as Strang splitting), the scheme is only first order in time for 2D problems. The time accuracy can be improved by using several stage Runga–Kutta schemes.

5. NUMERICAL RESULTS

The scheme described in Section 3 is tested on a variety of one- and two-dimensional problems. The first test problem is Woodward and Colella's blast wave problem [19] in which a complex set of strong shock, contact, and rarefaction waves interacts in a small closed region bound with reflective walls. Initially, the region is divided into the left, center, and right regions and the following initial conditions are assumed: $B = 0$, $V = 0$, $\rho = 1$ and $P_L = 1000$, $P_C = 0.01$, $P_R = 100$. A grid of 400 points with $\Delta t/\Delta x = 0.016$ is used and the density plots are shown in Fig. 1 at time steps 250, 400, 650, 700, 800, and 950. Comparing with previous results [19, 20] it is clear that the scheme described here performs very well and it produces rather sharp discontinuities with no spurious oscillations.

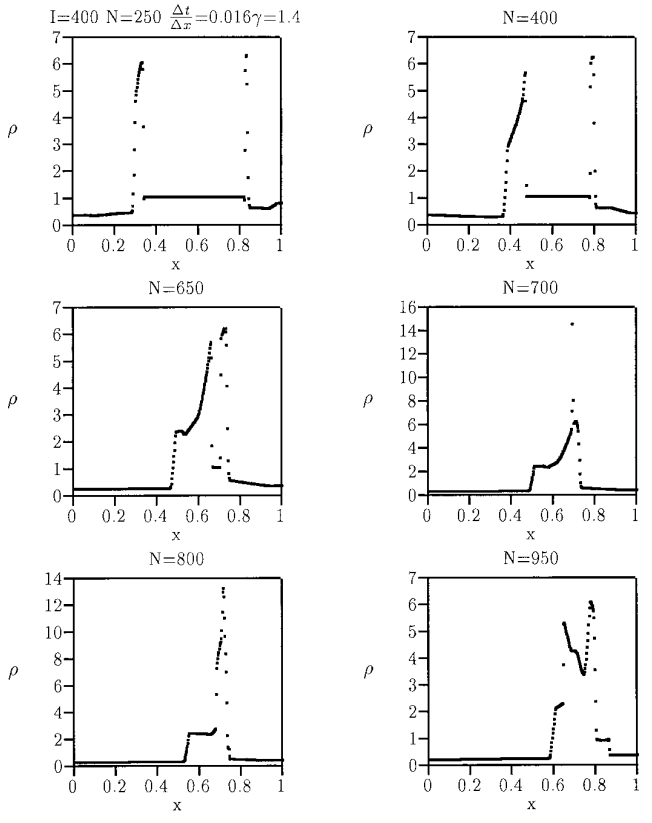

FIG. 1. The density plots for the Blast Wave problem.

The next one-dimensional test case is a purely hydrodynamic ($B = 0$) Sod's shock tube problem [21]. In this problem, a stationary ($V = 0$) monoatomic gas $\gamma = 1.4$ is initially separated into two regions with a diaphragm. The density and pressure on the left and right are given by $\rho_L = 1$, $P_L = 1$ and $\rho_R = 0.125$, $P_R = 0.1$, respectively. After the diaphragm is removed at $t = 0$, the characteristics will find their way into propagating on the x–t plane and producing a self-similar solution with a right moving shock followed by a contact and a left moving rarefaction wave. With a uniform mesh of 100 points, and with $\Delta t/\Delta x = 0.411$, the solution for the velocity and density after 35 time steps is shown in Fig. 2 with no postshock oscillations and rather sharp shock and contact discontinuity, a nice feature of the modified Superbee limiter.

The performance of the new sonic fix is checked with Roe's sonic test problem [5] where the initial conditions are $B = 0$, $V = 0$, $\rho_L = P_L = 100$, and $\rho_R = P_R = 1$ with

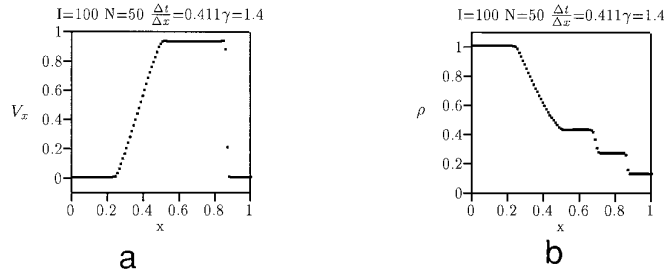

FIG. 2. The velocity and density plots for Sod's shock tube problem.

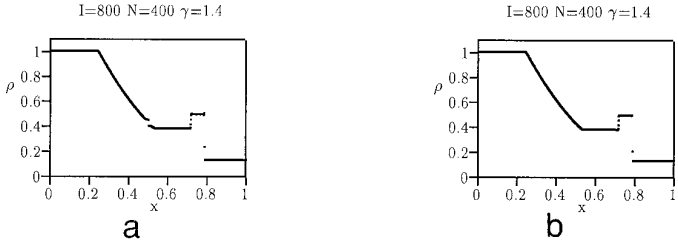

FIG. 4. The density plots for Brio's high-Mach MHD problem. (a) Without a sonic fix and (b) with the new sonic fix.

$\gamma = 1.4$. The same mesh and $\Delta t/\Delta x = 0.2$ are taken and the results for density without and with the new sonic fix are shown in Fig. 3. Without the sonic fix (Fig. 3a), the scheme leads to a noticeable expansion shock even though the contact and the shocks are very well resolved. Figure 3b shows the result with the new sonic fix where the expansion shock is totally eliminated.

The next test problem is a high-Mach-number problem introduced for MHD by Brio and Wu [22]. The initial conditions are given by $W_{\mathrm{L}} = [1, 0, 0, 0, 0, \sqrt{4\pi}, 0{,}1000]$ and $W_{\mathrm{R}} = [0.125, 0, 0, 0, 0, -\sqrt{4\pi}, 0, 0.1]$ with $\gamma = 1.4$, where W is the primitive state defined as $W = [\rho, V_x, V_y, V_z, B_x, B_y, B_z, P]$. A grid of 800 points is taken and the results for the density without and with the new sonic fix are displayed in Fig. 4 at $t = 0.0063$. Again, the results are excellent and the new sonic fix works successfully for the MHD as well. Figure 5 shows the normalized magnitude of the transferred quantity for the x momentum at the sonic interface. This value is related to Eq. (14) and decays in time as expected.

The first two-dimensional test problem is the unsteady flow of a monoatomic gas (with $\gamma = 1.4$) over a step with Mach 3 inflow. The domain is a rectangle with a length of 3 and a height of 1. The step with a height of 0.2 is placed at $x = 0.6$. The initial condition is $W = [1.4, 3, 0, 0, 0, 0, B_z, 1]$. The left and right boundaries are incoming and outgoing, respectively, and the upper and lower boundaries are reflective. Since the magnetic field is perpendicular to the plane, the divergence condition is automatically satisfied with a vanishing source in (61).

Figure 6 shows the result for the density contours with two different values of B_z. The case with $B_z = 0$ is a purely hydromagnetic problem with a triple Mach reflection, expansion corner, and a slip line near the upper surface. The new sonic fix works well for two dimensions since no expansion shock exists across the expansion corner. This is also a good test problem for checking the performance of the MHD codes in the limit as $B \to 0$. How the eigensystem of MHD equations should be modified for this limiting case to have it reduce to that of Euler's equations is explained by Aslan in [23, 24]. As seen from Fig. 6b, the strong perpendicular field ($B_z = 50$) acts like an isotropic magnetic pressure on the x–y plane, causing the bow shock move to front, leaving a disappearing slip line behind.

The next test problem is the blast wave in free space with an arbitrarily directed magnetic field. The blast wave is driven by a circular region ($r = 0.4$) with a large overpressure. The initial conditions are $\mathbf{v} = 0$, $\rho = 1$, $B_x = 30$, $P_{\mathrm{in}} = 100$, and $P_{\mathrm{out}} = 1$ with $\gamma = 1.4$. With these initial conditions, it is expected that the strong magnetic field in the x direction will give rise to anisotropy in the density and pressure. Figure 7 shows the results for the density and B_x contours at $t = 0.002$ on an 80×80 grid. The source is taken to be zero and the 7×7 MHD eigensystem is used. The graph for B_x shows a divergence error near

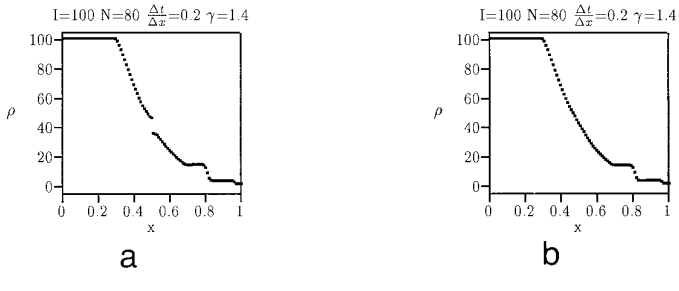

FIG. 3. The density plots for Roe's strong sonic problem. (a) Without a sonic fix and (b) with the new sonic fix.

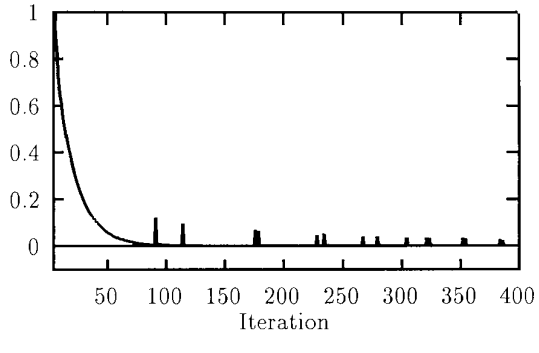

FIG. 5. The normalized magnitude of transferred flux for x momentum at the sonic interface.

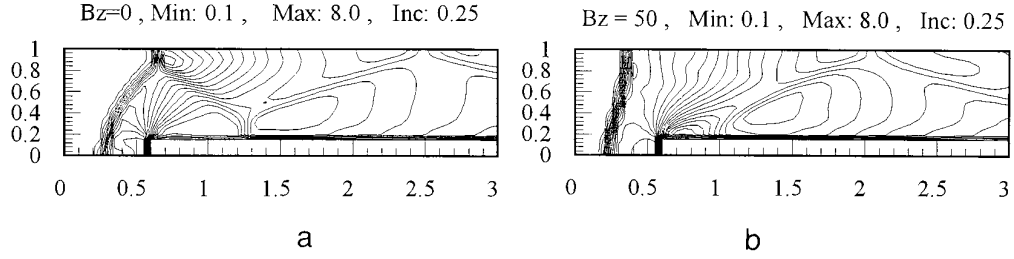

FIG. 6. The density contours for the MHD version of Mach = 3 flow over a step for (a) $B_z = 0$ and (b) $B_z = 50$.

the bottom, leading to the creation of unphysical magnetic monopoles. This error causes the MHD code to crash shortly after these magnetic monopoles are created. Figure 8 shows the results for $t = 0.04$ (running the code 20 times longer than in the previous case) on the same grid. In this case the source is retained and the 8×8 MHD eigensystem is used. The result is excellent since the production rate of the magnetic monopoles is reduced significantly. After the explosion, a rarefaction wave moves inward and a contact discontinuity and strong shock move outward. The existence of a strong horizontal field disturbs the symmetry, leading to stronger horizontal shock. It must be noted here that the new sonic fix also works well in the arbitrary magnetic field structure. The discontinuities are slightly degraded in two-dimensional problems due to the fact that the scheme is first-order accurate in time and no rotation is used in the Riemann solver. A rotated Riemann solver with quadrilateral and triangular cells for the solutions of MHD equations is being prepared and this will be the subject of subsequent papers.

The last test problem (whose analytical solution exists) was originally constructed such that a 29° reflected shock is the equilibrium solution across a Cartesian tube. The states at the left W_L and upper boundaries W_R are specified and the lower and right boundaries are taken as reflective and outgoing, respectively. To find the state on the right of the 29° shock, the R–H conditions are solved in the normal direction provided that the left state is known. These states are given by

$$W_L = [1, 2.9, 0, 0, \sqrt{\pi}, 0, 0, 1/\gamma]^T$$
$$W_R = [1.460, 2.716, -0.405, 0, 2.424, -0.361, 0, 1.223]^T \quad (71)$$

with $\gamma = 1.4$. The solution includes a discontinuity in the magnetic field across the shock which leads to a surface current (in the z direction) flowing along the infinitesimally thin layer of the shock. This problem is solved on a Cartesian grid with x:[0, 2], y:[0, 1] and the left state is assumed throughout the grid as the initial condition. It is expected that the time-dependent problem reaches the defined equilibrium state (71) with the divergence condition on the magnetic field preserved. Since the solution is known analytically, this is a very good test problem for checking the accuracy and performance of any numerical method in solving the MHD equations. Figure 9a shows the resulting B_x contours obtained with a 7×7 eigensystem (no divergence wave) and no $\nabla \cdot \mathbf{B}$ source. A 50×25 grid is used along with entropy satisfying second-order fluxes limited by a modified Superbee limiter. When the divergence cleaning is not done, using the 7×7 eigensystem is invalid in multidimensional MHD. As seen from Figure 9a, nonphysical magnetic islands on each side of the shock occurred. Once these islands are formed, nonphysical mag-

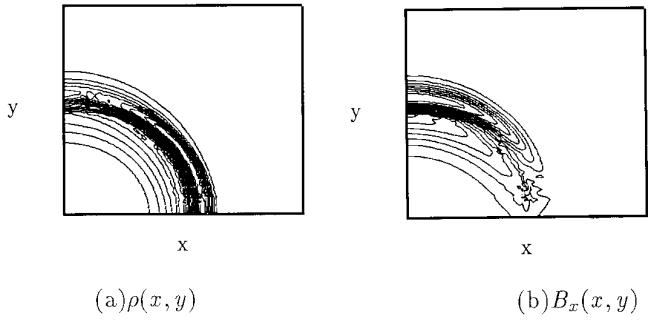

FIG. 7. The density and B_x contours for the blast wave in free space obtained with a vanishing source and the seven-wave MHD eigensystem.

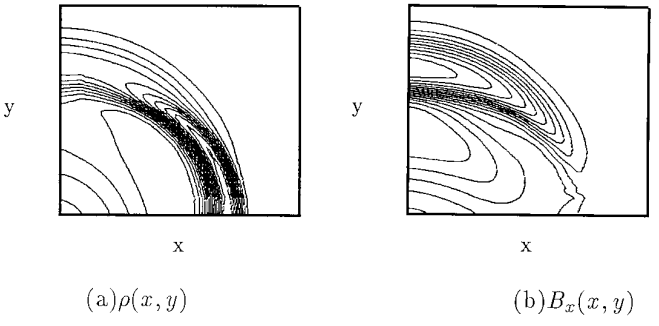

FIG. 8. The density and B_x contours for the blast wave in free space obtained with the divergence source and the eight-wave MHD eigensystem.

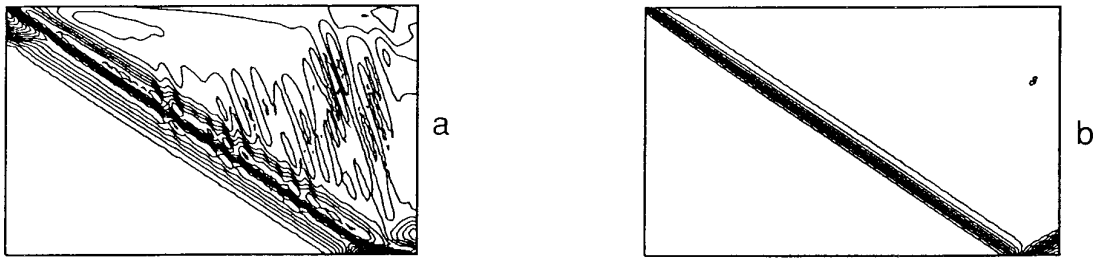

FIG. 9. Regular high-Mach reflection problem. B_x contours obtained by (a) a 7×7 eigensystem without the divergence source and (b) an 8×8 eigensystem with the source.

netic monopoles are created and the numerical iterations become unstable. Figure 9b gives the results on the same grid obtained with the 8×8 eigensystem and divergence source. As seen, the solution is excellent since there are no problems arising from the divergence condition and the shock compression remains uniform (even after reflection). As a remark, it is noted that using a rotated Riemann solver would improve these results which is the main objective of subsequent papers.

6. CONCLUSION

The solution of hyperbolic equations with simple first-order upwind differencing produces errors that accumulate in time and it produces unphysical expansion shocks which slow down the convergence. To handle this problem, a new sonic fix that utilizes a dissipation term which is directly embedded in the fluxes is described here. The fix is not empirical but certainly relies on physical grounds producing the correct decay rate of sonic gradients. A new implementation of the source terms into the flux limiters is also discussed in detail. A wide variety of one- or two-dimensional test problems resulting from the solutions of Euler's equations and a new implementation of a recently introduced scheme for the MHD equations are presented. The results show that the scheme with the new sonic fix along with new source strengths is robust and accurate, producing rather sharp contact discontinuities and shocks without spurious oscillations. The scheme is currently being improved to include curvilinear geometries, quadrilateral grids with flux rotation, and triangular grids.

ACKNOWLEDGMENTS

The support from NATO Collaborative studies (CRG-941130) is acknowledged. This work is also supported by the NSF under Contract INT95-148148 with the University of Michigan. The discussions with P. Roe, B. van Leer, and K. Powell are gratefully acknowledged.

REFERENCES

1. A. Harten, High-resolution schemes for hyperbolic conservation laws, *J. Comput. Phys.* **49,** 235 (1983).
2. P. K. Sweby, High-resolution schemes using flux limiters for hyperbolic conservation laws, *SIAM J. Numer. Anal.* **21,** 995 (1984).
3. B. van Leer, W. T. Lee, and K. G. Powell, Sonic point capturing (AIAA Paper 89-1945), *AAIA J.* **49,** 235 (1983).
4. R. J. LeVeque, High-resolution finite volume methods on arbitrary grids via wave propagation, *J. Comput. Phys.* **78,** 36 (1988).
5. P. L. Roe, Sonic flux formulae, *SIAM J. Sci. Statist. Comput.* **13,** 611 (1992).
6. N. Aslan, *Computational Investigations of Ideal MHD Plasmas with Discontinuities,* Ph.D. thesis (Nuclear Engineering Department, University of Michigan, 1993).
7. A. Zachary and P. Colella, A higher-order Godunov method for the equations of ideal magnetohydrodynamics, *J. Comput. Phys.* **99,** 341 (1992).
8. Glaister, *An Approximate Riemann Solver for Compressible Flows with Axial Symmetry,* Num. Anal. Report, 2/87 (Department of Mathematics, University of Reading, 1987).
9. W. F. Noh, Errors for calculations of strong shocks using an artificial viscosity and an artificial heat flux, *J. Comput. Phys.* **72,** 78 (1978).
10. P. L. Roe, Characteristic-based schemes for the Euler equations, *Annu. Rev. Fluid Mech.* **18,** 337 (1986).
11. P. L. Roe, Approximate Riemann solvers, parameter vectors, and difference schemes, *J. Comput. Phys.* **43,** 357 (1981).
12. N. Aslan, Numerical solutions of one-dimensional MHD equations by a fluctuation approach, *Int. J. Numer. Methods Fluids* **22,** 569 (1996).
13. R. J. LeVeque, Numerical methods for conservation laws, *Lectures at ETH Zurich* (1989).
14. Philip L. Roe, Some contributions to the modelling of discontinuous flows, *Lectures Appl. Math.* **22,** 163 (1985).
15. N. Aslan and T. Kammash, Plasma dynamics in a magnetically insulated target for inertial fusion, *Fusion Technol.* **26,** 184 (1994).
16. J. U. Brackbill and D. C. Barnes, The effect of nonzero $\nabla \cdot \mathbf{B}$ on the numerical solution of the magnetohydrodynamic equations, *J. Comput. Phys.* **35,** 426 (1980).
17 K. G. Powell, *An Approximate Riemann Solver for Magnetohydrodynamics* (*That Works in More Than One Dimension*), ICASE Report No. 94-24 (Langley, VA, 1994).
18. T. I. Gombosi, K. G. Powell, and D. L. De Zeeuw, Axisymmetric modelling of cometary mass loading on an adaptively refined grid, *J. Geophys. Res.* **99,** A11, 21525 (1994).
19. P. Woodward and P. Colella, The numerical solution of two-dimensional fluid flow with strong shocks, *J. Comput. Phys.* **54,** 115 (1984).
20. W. J. Rider, A review of approximate Riemann solvers with Godunov's method in Lagrangian coordinates, *Comput. Fluids* **23,** 397 (1994).

21. G. Sod, A survey of several finite difference methods for systems of hyperbolic conservation laws, *J. Comput. Phys.* **27,** 1 (1978).
22. M. Brio and C. C. Wu, An upwind differencing scheme for the equations of ideal magnetohydrodynamics, *J. Comput. Phys.* **75,** 400 (1988).
23. N. Aslan, Numerical solutions of 2-D MHD equations by finite volume method with quadrilateral cells, in *Proceedings, Ninth Int. Conf. in Numerical Meth. in Laminar and Turbulent Flow, 1995,* 9-2, 1633.
24. N. Aslan, Two dimensional solutions of MHD equations with adapted Roe's method, *Int. J. Numer. Methods Fluids* **23,** 1 (1996).